Hydrol. Earth Syst. Sci., 12, 1027–1037, 2008
www.hydrol-earth-syst-sci.net/12/1027/2008/

Hydrology and Earth System Sciences

An integrated model for the assessment of global water resources – Part 2: Applications and assessments

N. Hanasaki[1], **S. Kanae**[2], **T. Oki**[2], **K. Masuda**[3], **K. Motoya**[4], **N. Shirakawa**[5], **Y. Shen**[6], **and K. Tanaka**[7]

[1]National Institute for Environmental Studies, Japan
[2]Institute of Industrial Science, University of Tokyo, Japan
[3]Frontier Research Center for Global Change, Japan
[4]Faculty of Education and Human Studies, Akita University, Japan
[5]Graduate School of Systems and Information Engineering, University of Tsukuba, Japan
[6]Center for Agricultural Resources Research, The Chinese Academy of Sciences, China
[7]Disaster Prevention Research Institute, Kyoto University, Japan

Received: 17 September 2007 – Published in Hydrol. Earth Syst. Sci. Discuss.: 2 October 2007
Revised: 7 May 2008 – Accepted: 30 June 2008 – Published: 29 July 2008

Abstract. To assess global water resources from the perspective of subannual variation in water availability and water use, an integrated water resources model was developed. In a companion report, we presented the global meteorological forcing input used to drive the model and six modules, namely, the land surface hydrology module, the river routing module, the crop growth module, the reservoir operation module, the environmental flow requirement module, and the anthropogenic withdrawal module. Here, we present the results of the model application and global water resources assessments. First, the timing and volume of simulated agriculture water use were examined because agricultural use composes approximately 85% of total consumptive water withdrawal in the world. The estimated crop calendar showed good agreement with earlier reports for wheat, maize, and rice in major countries of production. In major countries, the error in the planting date was ± 1 mo, but there were some exceptional cases. The estimated irrigation water withdrawal also showed fair agreement with country statistics, but tended to be underestimated in countries in the Asian monsoon region. The results indicate the validity of the model and the input meteorological forcing because site-specific parameter tuning was not used in the series of simulations. Finally, global water resources were assessed on a subannual basis using a newly devised index. This index located water-stressed regions that were undetected in earlier studies. These regions, which are indicated by a gap in the subannual distribution of water availability and water use, include the Sahel, the Asian monsoon region, and southern Africa. The simulation results show that the reservoir operations of major reservoirs ($>1\,\mathrm{km}^3$) and the allocation of environmental flow requirements can alter the population under high water stress by approximately -11% to $+5\%$ globally. The integrated model is applicable to assessments of various global environmental projections such as climate change.

Correspondence to: N. Hanasaki
(hanasaki@nies.go.jp)

1 Introduction

Previous assessments of global water resources have projected current and future global water stress, focusing mainly on the spatial, rather than temporal, distribution of water availability and water use. A typical approach is to display the global distribution of per capita annual water availability (Arnell, 1999; Arnell, 2004) or the withdrawal to availability ratio on an annual basis (Vörösmarty et al., 2000; Oki et al., 2001; Alcamo et al., 2003a; Alcamo et al., 2003b). However, seasonality in both water availability and water use occurs in some parts of the world. Therefore, subannual variability must be taken into account. In this two-part report, we introduce an integrated global water resources model and assess global water resources through the application of the model from the perspective of subannual variation. Here, we addressed the following key question: Given that earlier global water resources assessments were on annual basis, does the assessment of water resources on a subannual basis reveal any water-stressed regions that were previously overlooked by annual assessments?

Published by Copernicus Publications on behalf of the European Geosciences Union.

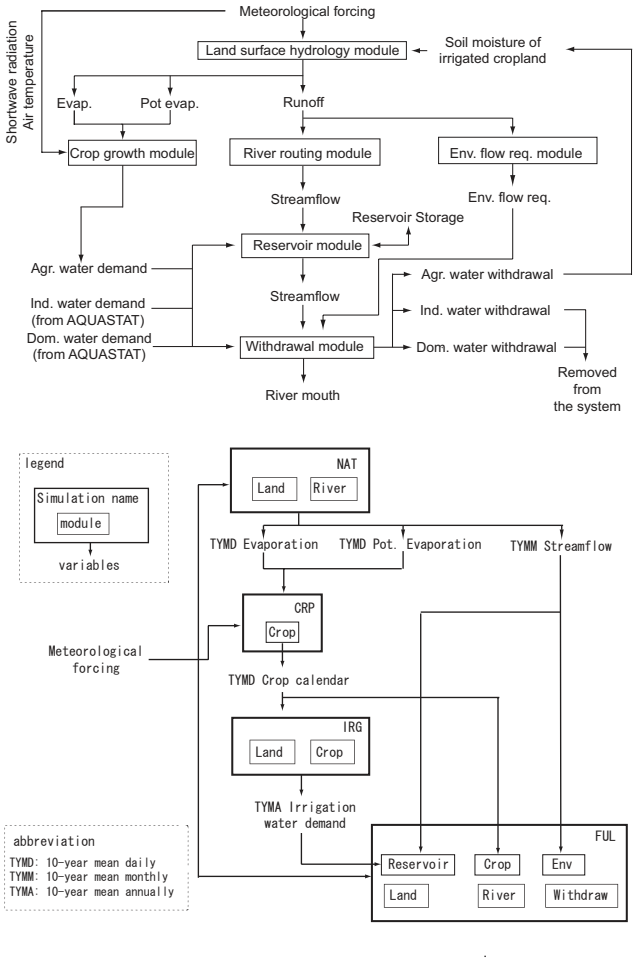

Fig. 1. Schematic diagram of **(a)** water flow among the modules and **(b)** the simulation.

We developed an integrated global water resources model with six modules: land surface hydrology, river routing, crop growth, reservoir operation, environmental flow requirements, and anthropogenic water withdrawal. The model simulates both natural and anthropogenic water flow globally (excluding Antarctica) at a spatial resolution of $1^\circ \times 1^\circ$ (longitude and latitude). The companion report (Hanasaki et al., 2008) presents the integrated model and the global meteorological forcing inputs that drive the model. Here, we present model applications and discuss the results of global water resources assessments using the integrated model. The input data and simulation design are described (Sect. 2). Some key estimations of water use are then validated (Sect. 3). Finally, the results of the global water resources assessment are presented (Sect. 4) and discussed (Sect. 5).

Table 1. List of input global geographical data.
The spatial resolution is $1^\circ \times 1^\circ$ (latitude and longitude).

Variable	Note/Reference
Albedo	Hall et al., 2006 (ISLSP2)
Cropland area	Ramankutty and Foley, 1998
Irrigated area	Döll and Siebert, 2000
Crop type	Leff et al., 2004
River network	Oki and Sud, 1998 (TRIP)
Vegetation	Globally uniform (bulk transfer coefficient: 0.003)
Soil type	Globally uniform (depth: 1 m, field capacity: 0.30 m^3/m^3, wilting point: 0.15 m^3/m^3)

2 Simulation

2.1 Input data

To drive the integrated model, we used the meteorological forcing input F-GSWP2-B1, which is described in detail in the companion paper (Hanasaki et al., 2008). It consists of seven variables: air temperature, specific humidity, wind speed, air pressure, downward shortwave radiation, downward longwave radiation, and precipitation. All variables are three-hourly from 1 January 1986 to 31 December 1995 at a spatial resolution of $1^\circ \times 1^\circ$. The meteorological forcing input is a hybrid product of ground observation-based monthly gridded data and temporally high-resolution reanalysis data. In addition to the meteorological forcing input, we used various geographical data (Table 1). The use of these data in the six modules is described in Part 1 (Hanasaki et al., 2008).

2.2 Integration of simulations

To run the fully coupled global water resources model, a series of simulations is required (Fig. 1a). First, the land surface hydrology module and the river routing module were coupled, and a global natural hydrological simulation was conducted for 10 years from 1986 to 1995 (hereafter "NAT simulation", short for natural hydrological cycle simulation). The purpose of this simulation was to obtain mean hydrological variables. These items included mean annual streamflow for the reservoir operation module, mean monthly runoff for the environmental flow requirement module, and mean daily evaporation and potential evaporation to estimate the crop calendar.

Second, a global cropping calendar was estimated by conducting a special simulation using the crop growth module (hereafter "CAL simulation," short for crop calendar estimation simulation). In this simulation, four hydrometeorological inputs were used: mean daily air temperature, shortwave radiation, evapotranspiration, and potential

evapotranspiration. The latter two variables were obtained from the NAT simulation. After this, 365 sets of crop yield were calculated for each grid by shifting the starting date of cropping from 1 January to 31 December, and the cropping date that produced the largest yield in a year was determined. The crop yield was estimated by the crop growth module based on concepts of heat unit theory, potential biomass, and a harvest index (e.g., temperature, shortwave radiation, and water during a cropping period determine crop yield). If the temperature in the cropping period fell below the base temperature (see Sect. 3.3 and Appendix D of Hanasaki et al., 2008), the crop died and the crop yield was zero, except for winter crops. The cropping calendar for double crops was also estimated for the remaining noncropping period so as not to overlap the planting to harvesting period of the first crop. The minimum interval between two cropping periods was set at 15 days. This simulation was conducted for all 19 types of crops (18 specific crop types and one generic crop parameter).

Third, a simulation was conducted to estimate irrigation water demand. The land surface hydrology and crop growth modules were coupled, and a global hydrological simulation was conducted for 10 years from 1986 to 1995 (hereafter "IRG simulation", short for ideally irrigated simulation). The irrigation water requirement was calculated from the deficit of soil moisture in irrigated fields during the cropping period (see Sect. 3.3 of Hanasaki et al., 2008). In this simulation, the irrigation water requirement was fully applied during the cropping period from an imaginary source of water. This amount of water corresponded to the consumptive irrigation water demand. Finally, all six modules were coupled, and global water resources were simulated from 1986 to 1995 (hereafter "FUL simulation," short for fully coupled simulation).

The six modules are coupled as follows (Fig. 1b). First, the land surface hydrology module is used to calculate energy and water balances on land surfaces. Next, the crop growth model is activated. The input shortwave radiation and air temperature are identical to those of the land surface hydrology module, and evaporation and potential evaporation are the simulated results of the land surface hydrology module. Consumptive agricultural water demand is estimated during the cropping period. Runoff is routed by the river routing model, and streamflow is calculated. This calculation is conducted from upper stream grids to lower stream grids; if reservoirs are geo-referenced in the calculated grid cells, the reservoir operation module calculates release, storage, and altered streamflow. The environmental flow module simulates the monthly environmental flow requirement from the monthly runoff. Finally, the anthropogenic water withdrawal module links water demand and streamflow. This module withdraws domestic, industrial, and agricultural water from streamflow in that order. Withdrawal is controlled to remain at or above the environmental flow requirement. The agricultural water that is withdrawn is added to the soil moisture of irrigated lands, and the domestic and industrial water that is withdrawn is removed from the integrated model system (i.e., it disappears without the closure of water and energy balances on the land surface). In reality, some portion of withdrawn water evaporates (water consumption) and the remaining portion returns to rivers or aquifers (return flow). For simplicity, the model takes only consumptive water use into account, and only the consumptive portion is withdrawn from the water source.

For all simulations, the meteorological input for the first year of the simulation period was iteratively given to the coupled model until soil moisture, river channel water storage, and reservoir storage reached equilibrium. A 10-year simulation was then conducted.

3 Validation

We validated the estimated crop calendar, irrigation water withdrawal, and environmental flow requirement and compared our results with those from earlier studies. The estimation of the timing and amount of the agricultural water requirement is critical in water resources assessment because agricultural water makes up 66% of the total water withdrawal and 85% of the total water consumption (Shiklomanov, 2000). The validation of the timing and volume of simulated water availability (i.e., runoff and streamflow) is described in Part I of this report (Hanasaki et al., 2008). The validation of the reservoir operation module is omitted because it has already been described elsewhere (Hanasaki et al., 2006). The withdrawal module is also omitted because it couples with the water fluxes of the five modules, but does not generate any new independent variables.

3.1 Crop calendar

The estimated crop calendar was compared with that reported by the World Agricultural Outlook Board of the US Department of Agriculture (1994; hereafter WAOB94), which provides the planting and harvesting dates of major crops for major countries of the world. We compiled planting dates and harvesting dates of three major grains, namely, wheat, maize, and rice, for 10 countries with the highest production in the world in 2000 (Food and Agriculture Organization, 2007a; Fig. 2). WAOB94 normally provides one general cropping calendar for a country, and both planting date and harvesting date have a wide range of up to four months.

Wheat is the most widely planted crop in the world (Ishii et al., 1999). Cropping can be roughly divided into two patterns: spring wheat, which is planted in spring and harvested in autumn; and winter wheat, which is planted in autumn and harvested in early summer (Fig. 2a). For spring wheat, both the simulated planting dates and harvesting dates in the USA, Canada, and Russia generally agreed with those of WAOB94. In China, both the planting date and the harvesting date were

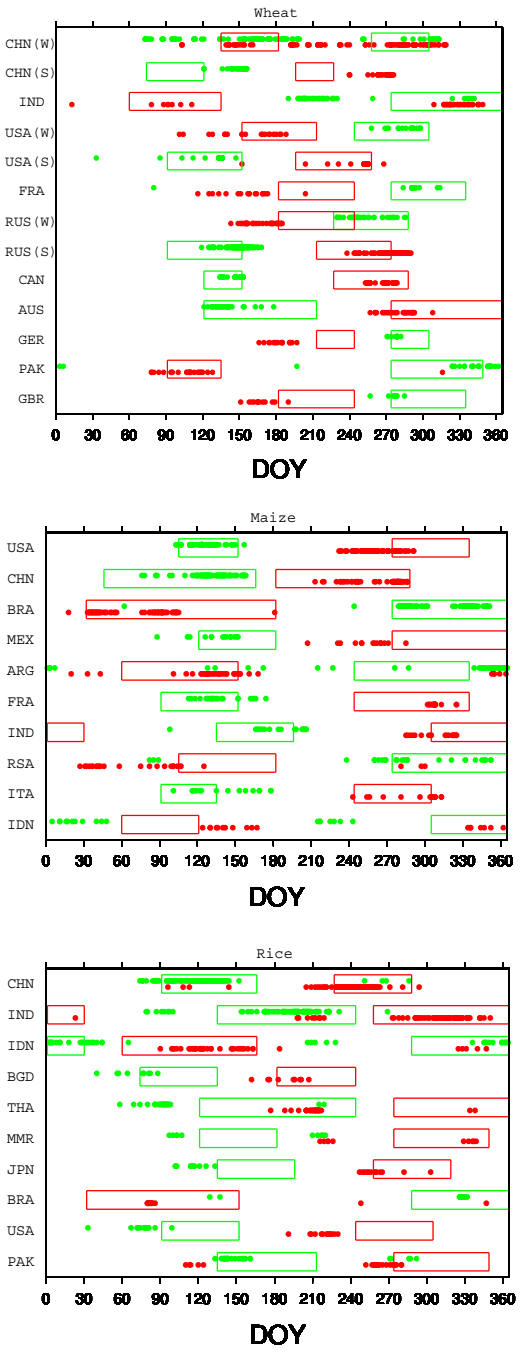

Fig. 2. Simulated planting and harvesting dates for **(a)** wheat, **(b)** maize, and **(c)** rice. The cropping calendars of 10 countries are shown for each crop with the largest production. Green plots show the simulated planting date for each grid; red plots show the harvesting date. Grids with $>100\,km^2$ of cropland with $>3\%$ of the cropland occupied by the species were selected. Green boxes show the observed planting period; red boxes show the harvesting period (World Agricultural Outlook Board US Department of Agriculture, 1994). In Fig. 2a, (W) denotes winter wheat, and (S) denotes spring wheat.

approximately 1 month later than those of the WAOB94. For winter wheat, the simulated planting dates were reproduced fairly well, except for China and India, whereas the simulated harvesting dates were sometimes 1 month (Russia, Britain) to 2 months (France, Germany) earlier than those of the WAOB94.

The planting dates of winter wheat in China and India were split into two groups: one resembled winter wheat and the other resembled spring wheat. This variation reflected differences in regional performance. In India, the simulated planting date of northwestern India agreed well with the observations, but in north central to northeastern India, the simulated planting date was 2–3 months earlier than in the WAOB94 and the harvesting date was before the arrival of winter. In China, the simulated planting date of the southern North China Plain was well simulated, but the remaining areas such as the Sichuan Basin and central North China Plain had a simulated crop calendar that resembled spring wheat; however, in reality, winter wheat was expected. These erroneous simulated planting periods were caused by water stress during the cropping period. In both China and India, low precipitation in winter restricted the crop yield of winter wheat to levels below those of spring wheat. We estimated the planting date under ideal water conditions (i.e., no water stress during the cropping period). In this case, the planting date was well reproduced (not shown). In these regions, the cropping calendar could be improved by irrigation. However, because the WAOB94 did not separate the crop calendar into irrigated and nonirrigated, we used the estimation with no irrigation. For maize, the planting dates in major cropping countries, namely, the USA, China, Brazil, and Mexico were well reproduced (Fig. 2b). Harvesting dates were also well reproduced in China and Brazil, but they were approximately 1 month earlier in the USA and Mexico.

More than 90% of rice is produced in the Asian monsoon region (Ishii et al., 1999). The simulated planting dates and harvesting dates were fairly captured in the 10 selected countries (Fig. 2c). In the top three countries, i.e., China, India, and Indonesia, both the planting date and harvesting date agreed with observations in most of these areas. There were exceptional grids with large differences from observations, but most of them were attributed to the vast climate region of these countries because they were at the margins of the major cropping areas. In Thailand and Myanmar, the planting date was estimated to be 1–2 months earlier and the cropping period was shorter than in WAOB94. In these countries, floodwater inundates paddy fields, but this process was not incorporated in our system.

In general, the planting dates and harvesting dates of major crops in major cultivation areas agreed with the WAOB94 dates. The error in simulated crop planting dates was less than ± 1 mo in major countries. Exceptions were winter wheat in China and India and rice in Thailand. There was a tendency toward the early estimation of harvesting dates, and the cropping periods were shorter than in

Table 2. Comparison of continental irrigation water withdrawal. Unit: $km^3\,yr^{-1}$.

Area (year)	This study (1995)	Döll and Siebert, 2002[1] (1995)	FAO, 2007 (2001)	Shiklomanov, 2000 (1995)
Asia	2140	1880	1940	1790
Europe	160	120	130	170
Africa	140	140	180	140
North America	240	190	200	200
South America	120	100	190	180
Oceania	20	30	20	20
Globe	2810	2450	2660	2500

1: Used in the global water resources assessment by Alcamo et al. (2003b).

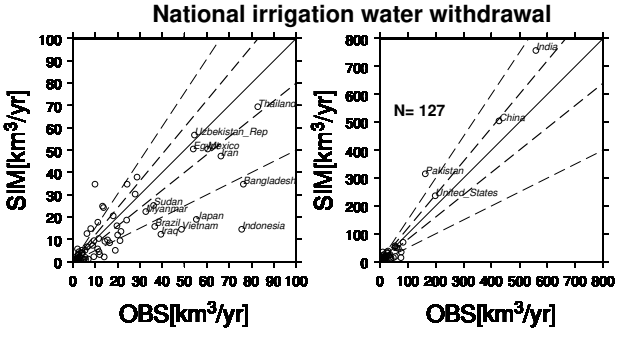

Fig. 3. Simulated irrigation water withdrawal for each country. The horizontal axis shows the reported value (Food and Agriculture Organization, 2007b) and the vertical axis shows the simulated value. The left panel shows countries with irrigation water withdrawal $<100\,km^3\,yr^{-1}$, and the right panel shows all plots.

WAOB94. This tendency was noticeable in countries that have warmer climates such as India, Brazil, and southeastern Asian countries, rather than those that have colder climates such as European countries. Air temperature is an important indicator to narrow down the potential cropping period, although in warmer countries, air temperature remains above the base temperature throughout the year and cannot be used as an indicator.

3.2 Irrigation water demand

The crop growth module estimated the consumptive water requirement (the IRG simulation), but most of the available statistics reported water withdrawal, which includes loss during delivery and return flow to the river channel or the recharge of groundwater. We used the methodology of Döll and Siebert (2002) to convert the consumptive water use requirement ($Q_{\mathrm{consumptive}}$) to a withdrawal basis ($Q_{\mathrm{withdrawal}}$). They defined the irrigation efficiency (k_{eff}; range from 0 to 1) as

$$k_{\mathrm{eff}} = Q_{\mathrm{consumptive}} \big/ Q_{\mathrm{withdrawal}} \quad (1)$$

They compiled k_{eff} for 19 countries and regions worldwide. It ranges from 0.35 to 0.70, reflecting irrigation facilities and practices. Previous estimates of global total irrigation water withdrawal ranged from $2450\,km\,yr^{-1}$ to $2660\,km\,yr^{-1}$ (Table 2). Our estimation of $2810\,km\,yr^{-1}$ slightly exceeds the upper limit of this range, but is still reasonable.

A country-based comparison of irrigation water withdrawal with the AQUASTAT database (Food and Agriculture Organization, 2007b) for 127 countries is provided (Fig. 3). Among countries with irrigation water withdrawal $>100\,km^3\,yr^{-1}$, water withdrawal in China and the USA was reproduced well and was within the range of ±20%. That in India was overestimated at slightly more than +20%, and that in Pakistan was overestimated considerably at almost twice the expected value. Countries with irrigation water demand between $30\,km^3\,yr^{-1}$ and $100\,km^3\,yr^{-1}$ can be categorized into two groups: Asian monsoon countries, i.e., Thailand, Bangladesh, Indonesia, Japan, Vietnam, and Myanmar; and the remaining countries, i.e., Iran, Mexico, Uzbekistan Republic, Egypt, Iraq, Brazil, and Sudan. Irrigation water withdrawal for the Asian monsoon countries was significantly underestimated, except for Thailand and Myanmar. It is interesting that these countries are all major rice producing countries (see Fig. 2c). In irrigated paddy rice fields, extra water may be used by farmers to enhance crop growth and to avoid weeds and low-temperature stress (Ishii et al., 1999), which was not included in the model. Except for Asian monsoon countries, three of seven countries came within ±20% of the expected value, and five of seven countries came within ±50%. Taking into account the limited reliability of available irrigation information, we judged the estimates to be tolerable. The error in simulated irrigation water withdrawal was less than ±50% in 10 of the 17 counties that withdraw $>30\,km^3\,yr^{-1}$.

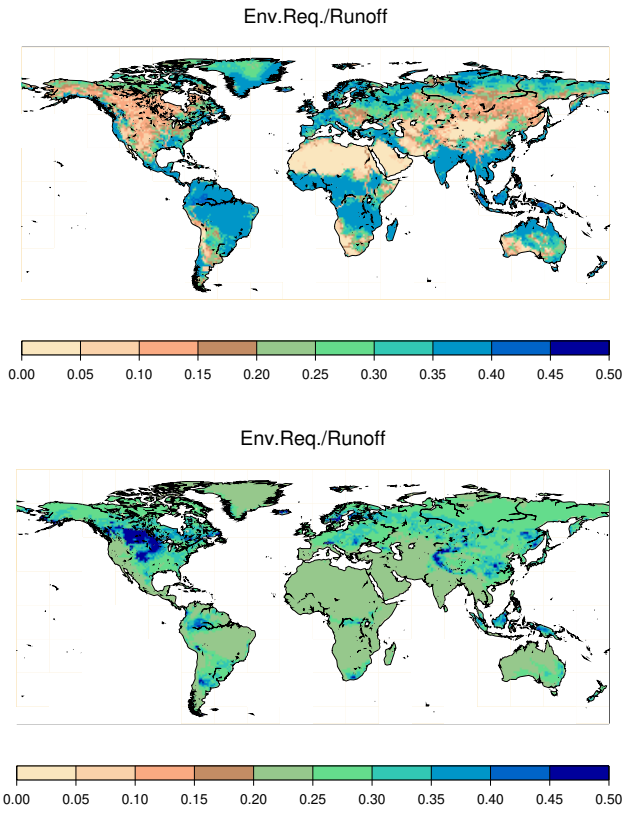

Fig. 4. Distribution of the ratio of estimated annual environmental flow requirement to annual total runoff (both grid-based). **(a)** This study and **(b)** Smakhtin et al. (2004).

3.3 Environmental flow requirement

Because there are no observations of environmental flow requirements, the estimated results of the environmental flow requirement module were compared with those reported by Smakhtin et al. (2004). Using the simulated streamflow of the NAT simulation, two annual environmental flow requirements were simulated using the environmental flow requirement module and the methodology of Smakhtin et al. (2004; Fig. 4). The simulated environmental flow requirement ranged from 0% to 40% of the total mean annual runoff (Fig. 4a). The minimum of 0% was allocated if the monthly runoff fell below 1 mm mo^{-1} throughout a year, which occurred mainly in arid areas (see Sect. 3.5 of Hanasaki et al., 2008) for a description of the environmental flow allocation algorithm). The maximum of 40% was allocated if the monthly runoff exceeded 10 mm mo^{-1} throughout a year. The total environmental flow requirement was estimated at 12 492 km^3 yr^{-1}, approximately 32% of the global total runoff of the NAT simulation. The global distribution pattern of the environmental flow requirement was quite similar to that of runoff.

In contrast, Smakhtin et al. (2004) reported quite a different global distribution of environmental flow requirements; for most regions of the world, the environmental flow requirement ranged between 20% and 30% of the mean annual runoff. The low regional variation was inherent in their classification and allocation of environmental flow requirements. The total environmental flow requirement was 10 682 km^3 yr^{-1}, approximately 27% of the global total runoff. The results clearly show that the method that we used (Shirakawa, 2004; Shirakawa, 2005) produced less environmental flow in arid to semi-arid areas and more in tropical areas. Our distribution (Fig. 4b) is different from that of Smakhtin et al. (2004) because the former was calculated from the runoff of the NAT simulation, whereas the latter used the simulated streamflow data of Döll et al. (2003; i.e., both the input meteorological data and hydrological model are different in our study). The environmental flow at high latitudes of North America was much higher in Smakhtin et al. (2004). The hydrological model of Döll et al. (2003) had a natural lake scheme, which buffered the fluctuation in runoff. The natural lakes that are abundant in northern North America enlarged the $Q90$ and the environmental flow requirement calculated by the algorithm of Smakhtin et al. (2004).

4 Water resources assessment

A global water resources assessment was conducted using indices. The three indices applied were the withdrawal to availability ratio, the cumulative withdrawal to water demand ratio, and the consumption to $Q90$ ratio.

4.1 Conventional index

First, the withdrawal to availability ratio (hereafter WWR) was calculated as the ratio of annual water withdrawal to annual runoff (renewable freshwater). It was expressed as

$$\mathrm{WWR}=\frac{W}{Q} \tag{2}$$

where W is the annual total withdrawal and Q is the annual streamflow. The areas with WWR$<$0.2 had low or no stress; areas with 0.2$\leq$WWR$<$0.4 had medium stress; and areas with 0.4$\leq$WWR had high stress (Raskin et al., 1997). To exclude sparsely populated deserts, grids with $<$1 person km^{-2} were masked out of the global distribution of WWR (Fig. 5a). The medium- to high-water-stressed regions extended from western India across the Middle East, northern Africa, the western Great Plains of the USA, and northern China to central Asia. This distribution largely agreed with that of earlier studies (e.g., Vörösmarty et al., 2000; Alcamo et al., 2003a; Alcamo et al., 2007; Oki and Kanae, 2006), indicating that global water availability and water use are well reproduced in our modeling system on an annual basis. The population living in water-stressed areas (0.4$\leq$WWR; the stressed population) was estimated to be 1250×10^6, which is smaller

than estimates by earlier studies (1760×10^6 by Vörösmarty et al., 2000; 1700×10^6 by Oki et al., 2001; 2279×10^6 by Alcamo et al., 2007). There are three major reasons for this difference. First, the input meteorological forcing and model were different in each study. Second, the spatial resolution of our study was lower than that of earlier studies, and consequently, both the population density and water use intensity were lower. Third, a large area of coastal zone was classified as sea in this simulation because of the characteristics of the land–sea mask of GSWP2. The world population on the land grid was 5195×10^6 in the simulation, but was reported as 5646×10^6 by the Center for International Earth Science Information Network (CIESIN) Columbia University and Centro Internacional de Agricultura Tropical (CIAT), 2005). Not only was the total population smaller, but the population density was higher in coastal zones. As a result, the stressed population was lower than in earlier studies.

4.2 Newly developed index

Previous studies have widely used the WWR, but little information is available regarding the temporal distribution of water availability and use within a year. Here, we propose a new index, the "cumulative withdrawal to demand ratio" (CWD) to express whether water demand is fulfilled on a subannual basis:

$$\mathrm{CWD}=\sum_{Y=1986}^{1995}\sum_{\mathrm{DOY}=1}^{365} w_{Y,\mathrm{DOY}} \Bigg/ \sum_{Y=1986}^{1995}\sum_{\mathrm{DOY}=1}^{365} d_{Y,\mathrm{DOY}} \qquad (3)$$

where $d_{Y,\mathrm{DOY}}$ is the daily water demand (Y: year; DOY: day of year), and $w_{Y,\mathrm{DOY}}$ is the simulated daily water withdrawal from streamflow for each grid. Daily water withdrawal does not exceed daily water demand ($w_{Y,\mathrm{DOY}}\leq d_{Y,\mathrm{DOY}}$). We set the area such that $0.8\leq$CWD indicates low or no stress, $0.5\leq\mathrm{CWD}<0.8$ denotes medium stress, and $\mathrm{CWD}\leq0.5$ represents high stress. These criteria were determined arbitrarily so that the highly stressed areas generally involve a well-established WWR. Figure 5b shows the distribution of the CWD index. Compared to WWR, water stressed regions were expansive. We examined the relationship between CWD and WWR for all land grids (total of 15,238; Fig. 6a). Of particular note are the plots in which WWR showed low water stress, but CWD showed high water stress. We defined category A as a WWR indicating low to no stress ($0\leq\mathrm{WWR}<0.2$) and CWD indicating medium to high stress ($0\leq\mathrm{CWD}<0.8$) or a WWR indicating medium stress ($0.2\leq\mathrm{WWR}<0.4$) and CWD indicating high stress ($0\leq\mathrm{CWD}<0.5$). Category A grids occur in the Sahel region, the Asian monsoon region, including India and Thailand, and southern Africa (Fig. 6c). In these regions, water stress is caused by a gap in the subannual distribution of water availability and water use, which has been overlooked in conventional studies based on WWR alone.

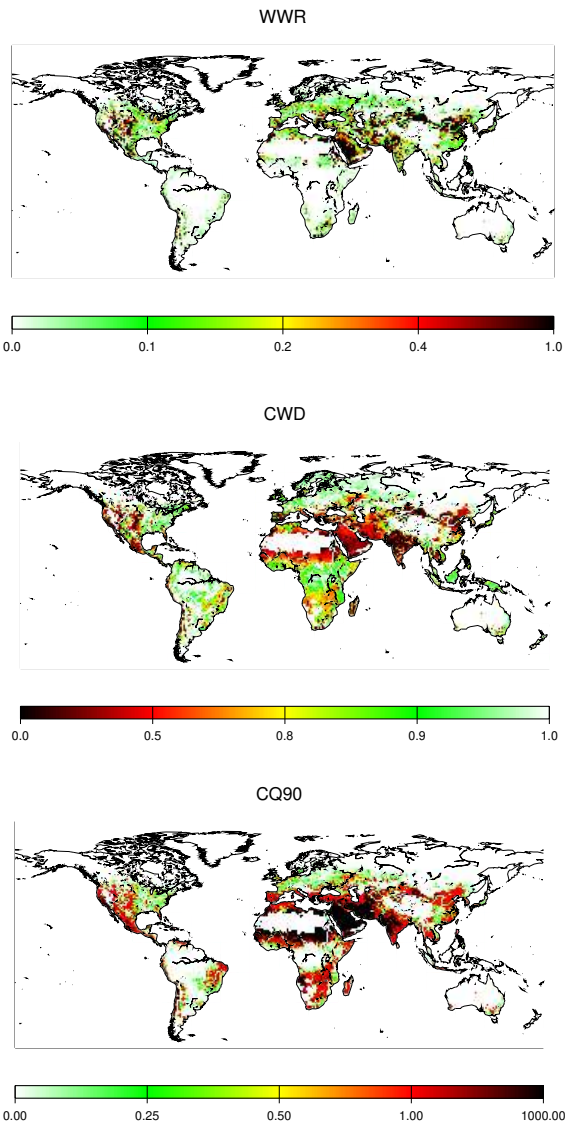

Fig. 5. Distribution of water-scarce areas. **(a)** Conventional withdrawal to water resources ratio (WWR; on an annual basis); **(b)** newly devised cumulative supply to demand ratio (CWD; on a daily basis); **(c)** consumptive water withdrawal to $Q90$ ratio ($CQ90$; on an annual basis). To distinguish water-scarce areas of highly populated areas from those of less populated areas (i.e., desert), grids with <1 person km^{-2} were eliminated from the calculations.

4.3 Consumption to $Q90$ ratio

The consumption to $Q90$ ratio (hereafter $CQ90$) was recently proposed by Alcamo et al. (2007) as

$$CQ90=\frac{C}{Q90} \qquad (4)$$

where C is consumptive water use and $Q90$ is the 90th percentile streamflow. They argued that this index is easier to interpret physically than WWR because $CQ90\geq1$

Table 3. Effects of reservoir operation and environmental flow on the population under water-stressed conditions. Unit: million people.

	Reservoir operation	Enabled	Enabled	Disabled	Disabled
	Environmental flow	Enabled	Disabled	Enabled	Disabled
High stress	CWD≤0.5	2420	2160	2540	2290
Medium stress	0.5<CWD≤0.8	870	790	920	870
Low/no stress	0.8<CWD	1880	2210	1710	2010

implies that the entire low monthly runoff in a river basin is depleted. This index takes the seasonality of water resources into account by using $Q90$ information. The estimated consumptive water requirement is largely exceeded in the water-stressed region indicated by the WWR, and the stressed region expands to eastern India, part of Southeast Asia, southern China, the Sahel, southern Africa, and eastern South America (Fig. 5c). The distribution is quite similar to that of CWD.

Although CWD (Fig. 5b) and $CQ90$ (Fig. 5c) show no clear differences in the distribution of water-stressed areas, CWD is more informative than $CQ90$. Figure 6b shows even the grid cells with $CQ90$ of 100 to 1000, which indicates that the consumptive water demand exceeds the $Q90$ by 100 to 1000 times, the CWD shows that there are lots of grid cells in the world in which approximately 80% of the daily water demand can be fulfilled. This clearly suggests that even $Q90$ is far below the annual average consumptive water use; if the water use is concentrated in water-rich periods, the availability can be quite high. The $CQ90$ indicates water-stressed regions with large seasonality in water availability; however, it provides little information when it exceeds 1. The CWD gives information on the potential availability of water with strong seasonality. The CWD may be more informative than the $CQ90$, such as, for example, in regional water resources assessments of the effect of the earlier arrival of streamflow peaks associated with climate change.

4.4 Effect of reservoirs and environmental flow requirements

How important are the operations of the 452 largest reservoirs and environmental flow from a global perspective? To answer this question we conducted three additional simulations. In the NORES simulation, the reservoir operation module was disabled; in the NOENV simulation, the environmental flow requirement module was disabled; and in the NORESENV simulation, both the reservoir operation module and environmental flow requirement module were disabled. Otherwise, the simulation settings were identical to those of the FUL simulation. The global water-stressed populations in terms of the CWD index were estimated for the FUL, NORES, NOENV, and NORESENV simulations (Table 3). The FUL simulation estimated a stressed population of 2420×10^6, whereas the NORES simulation increased the stressed population by 5% (2540×10^6) because the disabled reservoir operation decreased daily water availability. In contrast, the NOENV simulation decreased the stressed population by 11% (2160×10^6) because the disabled environmental flow requirement increased water availability. Finally, the NORESENV simulation decreased the population by 5% (2290×10^6). Thus, these factors can alter the population under high water stress by approximately -11% to +5% (Table 3), a range that is not negligible for water resources assessments.

5 Discussion

5.1 Uncertainty of important assumptions in water withdrawal

The water resources assessment was carried out under two important assumptions. The first assumption was that water is withdrawn only from river channels. In reality, groundwater, lakes, ponds, and glacial meltwater are major sources of water in some parts of the world. In addition, reservoirs $<10^9\,m^3$ that were not included in the model provide contributions. These nonriver water resources can be divided into renewable and nonrenewable components. For example, withdrawal from shallow groundwater, reservoirs, lakes, and ponds below the recharge rate is considered renewable. In contrast, withdrawal from deep groundwater and glacial meltwater and the overexploitation of lakes and ponds are considered nonrenewable. The renewable water resources were partly included in our simulation because the simulated runoff and streamflow are the result of water balance calculations on land surfaces, and the natural recharge of groundwater in lakes and ponds is implicitly included in the runoff. However, this does not apply to nonrenewable water resources, which were excluded from the simulation. Therefore, the simulated availability of water might be underestimated, especially in areas that rely heavily on nonrenewable water resources; the water use in these areas can be considered less sustainable and vulnerable to water scarcity.

The second assumption was that only water for consumptive use is withdrawn from river channels. In reality, a considerable amount of the withdrawn water does not reach the destination because of evaporation and percolation losses during delivery. Also, a considerable portion of the withdrawn water is returned to the river through drainage channels and groundwater flow. Consequently, the simulated water demand is underestimated. Part of the return flow is implicitly expressed by a simple subsurface flow scheme in the land surface module, and a portion of irrigated water is drained and returned to the river.

5.2 Uncertainty in modeling anthropogenic activities

Four major anthropogenic activities were modeled and implemented in the model. As stated in Part 1, we did not expect that the model could reproduce individual anthropogenic activities of the past; rather, we tried to reproduce the fundamental basis of these activities. Our modeling was based on the assumption that humans act simply and rationally. In some cases, anthropogenic activities in reality are wiser than were those in our model, and our simulation may have overestimated water stress. In contrast, in some cases, our modeled activities were too rational or too simple, and our simulation may have underestimated water stress. Further improvements of algorithms in the anthropogenic activity modules are needed for more realistic simulation.

6 Conclusions

An integrated water resources model was developed that consists of six modules to simulate both natural and anthropogenic water flows at daily intervals. Using the newly developed water resources model and the meteorological forcing input F-GSWP2-B1, global water availability and use were simulated for 10 years (1986–1995) at a resolution of $1^\circ \times 1^\circ$ (latitude and longitude). In this simulation, both the energy and water balances were closed in each grid cell. A global water resources assessment was conducted using a newly devised indicator, the cumulative withdrawal to demand ratio, which detected water-stressed regions that were previously overlooked. For example, a gap in the subannual distribution of water availability and water use was noted in the Sahel, the Asian monsoon region, and southern Africa. Even where annual water availability exceeds the annual water demand, because of uneven distribution, available water can fall below the demand in some periods in a year.

There are a number of potential applications for this model. First, it has applications for climate change impact assessment. Climate change is likely to alter future temperature and precipitation patterns and in turn alter the availability of renewable freshwater and water use. Earlier assessments used annually based water stress indicators such as per capita water availability. Arnell (2004) pointed out that

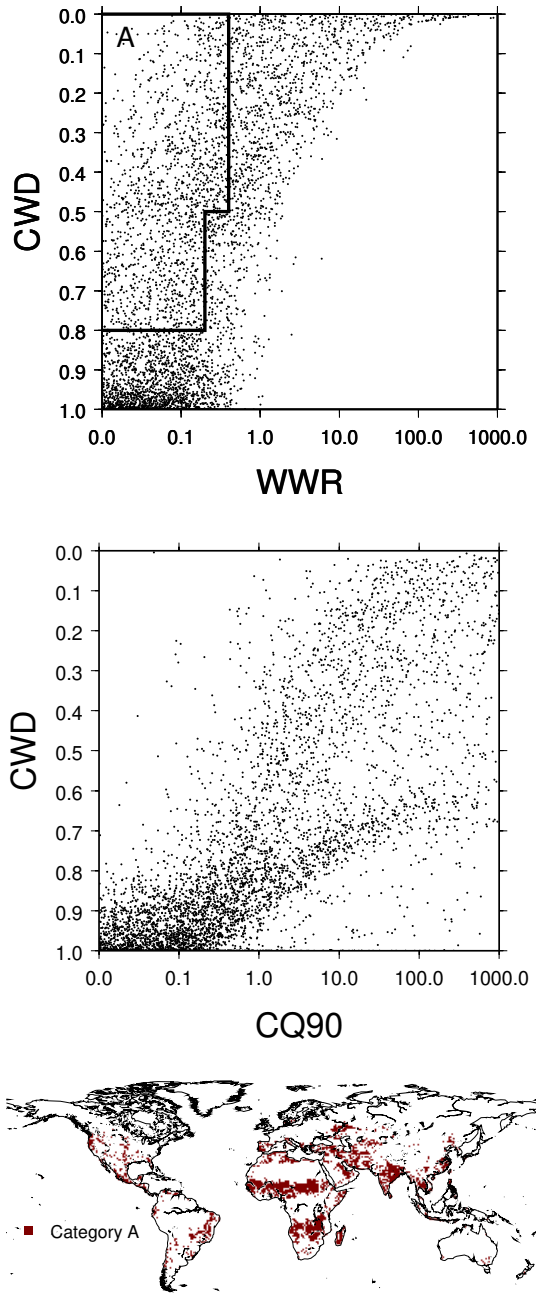

Fig. 6. (a) Scattergram showing the relationship between the withdrawal to water resources ratio (WWR) and the cumulative supply to water demand ratio (CWD) for all calculated grid cells (total of 15 238). Box A shows the plots in which WWR indicates low to no stress ($0 \leq \mathrm{WWR} < 0.2$) but CWD indicates medium to high stress ($0 \leq \mathrm{CWD} < 0.8$) or in which WWR indicates medium stress ($0.1 \leq \mathrm{WWR} < 0.4$) but CWD indicates high stress ($0 \leq \mathrm{CWD} < 0.5$). **(b)** Scattergram showing the relationship between the consumption to $Q90$ ratio ($CQ90$) and the cumulative withdrawal to water resources ratio (CWD). **(c)** Geographical distribution of the plots in box A.

according to this indicator, although increases in runoff tend to occur during high-flow seasons, climate change would appear to reduce global water stress. However, this is might not alleviate dry season problems if the extra water is not stored, and it would not ease water stress in other regions of the world (Kundzewicz et al., 2007). Our model and indicator (the cumulative withdrawal to demand) can assess the change in subannual variation in precipitation, runoff, and water use. A global water resources assessment under future global warming will be addressed in forthcoming papers.

Second, the model has applications for combined issues of food and water. Because the model can simulate crop water use in detail, it can be used to estimate virtual water (i.e., the volume of water that is used to produce goods and services; Hoekstra and Hung, 2002; Oki and Kanae, 2004). Furthermore, the crop growth module was used only to estimate crop calendars, but if we focus on the impact of water shortage to crop production during a cropping period, the simulated loss in crop production can serve as another water-stress index.

Acknowledgements. This study was supported by the Global Environmental Research Fund S-4 from the Ministry of the Environment, Japan, and a Grant-in-Aid for Scientific Research, (S)19106008, from the Japan Society for the Promotion of Science (JSPS). We thank two anonymous reviewers for helpful comments and suggestions.

Edited by: T. Wagener

References

Alcamo, J., Döll, P., Henrichs, T., Kaspar, F., Lehner, B., Rosch, T., and Siebert, S.: Development and testing of the WaterGAP 2 global model of water use and availability, Hydrolog. Sci. J., 48, 317–337, 2003a.

Alcamo, J., Döll, P., Henrichs, T., Kaspar, F., Lehner, B., Rosch, T., and Siebert, S.: Global estimates of water withdrawals and availability under current and future "business-as-usual" conditions, Hydrolog. Sci. J., 48, 339–348, 2003b.

Alcamo, J., Florke, M., and Marker, M.: Future long-term changes in global water resources driven by socio-economic and climatic changes, Hydrolog. Sci. J., 52, 247–275, 2007.

Arnell, N. W.: Climate change and global water resources, Global. Environ. Chang., 9, S31–S49, 1999.

Arnell, N. W.: Climate change and global water resources: SRES emissions and socio-economic scenarios, Global. Environ. Chang., 14, 31–52, 2004.

Center for International Earth Science Information Network (CIESIN) Columbia University, and Centro Internacional de Agricultura Tropical (CIAT): Gridded Population of the World Version 3 (GPWv3): Population Grids, Socioeconomic Data and Applications Center (SEDAC) Columbia University, Palisades, NY, 2005.

Döll, P. and Siebert, S.: A digital global map of irrigated areas, ICID J., 49, 55–66, 2000.

Döll, P. and Siebert, S.: Global modeling of irrigation water requirements, Water Resour. Res., 38, 1037, doi:10.1029/2001WR000355, 2002.

Döll, P., Kaspar, F., and Lehner, B.: A global hydrological model for deriving water availability indicators: model tuning and validation, J. Hydrol., 270, 105–134, 2003.

Food and Agriculture Organization: FAOSTAT, http://faostat.fao.org/, last access: 29 July 2008.

Food and Agriculture Organization: AQUASTAT, http://www.fao.org/ag/agl/aglw/aquastat/main/index.stm, last access: 29 July 2008.

Hall, F. G., de Colstoun, E. B., Collatz, G. J., Landis, D., Dirmeyer, P., Betts, A., Huffman, G. J., Bounoua, L., and Meeson, B.: ISLSCP Initiative II global data sets: Surface boundary conditions and atmospheric forcings for land-atmosphere studies, J. Geophys. Res.-Atmos., 111, D22S01, doi:10.1029/2006JD007366, 2006.

Hanasaki, N., Kanae, S., and Oki, T.: A reservoir operation scheme for global river routing models, J. Hydrol., 327, 22–41, 2006.

Hanasaki, N., Kanae, S., Oki, T., Masuda, K., Motoya, K., Shirakawa, N., Shen, Y., and Tanaka, K.: An integrated model for the assessment of global water resources - Part 1: Model description and input meteorological forcing, Hydrol. Earth Syst. Sci., 12, 1007–1025, 2008, http://www.hydrol-earth-syst-sci.net/12/1007/2008/.

Hoekstra, A. Y. and Hung, P. Q.: Virtual water trade, A quantification of virtual water flows between nations in relation to international crop trade, Institute of Hydraulic Engineering (IHE), Delft, The Netherlands, 2002.

Ishii, R., Nakaseko, K., and Takahashi, Y.: Agronomics, Asakura Publishing, Tokyo, Japan, 1999.

Kundzewicz, Z. W., Mata, L. J., Arnell, N. W., Döll, P., Kabat, P., Jiménez, B., Miller, K. A., Oki, T., Sen, Z., and Shiklomanov, I. A.: Freshwater resources and their management, in: Climate Change 2007: impacts, adaptation and vulnerability, contribution of working group II to the Fourth Assessment Report of the Intergovernmental Panel on Climate Change, edited by: Parry, M. L., Canziani, O. F., Palutikof, J. P., van der Linden, P. J., and Hanson, C. E., Cambridge University Press, Cambridge, UK, 173–210, 2007.

Leff, B., Ramankutty, N., and Foley, J. A.: Geographic distribution of major crops across the world, Global Biogeochem. Cy., 18, GB1009, doi:10.1029/2003GB002108, 2004.

Oki, T. and Sud, Y. C.: Design of total runoff integrating pathways TRIP – a global river channel network, Earth Interactions, 2, 1–37, 1998.

Oki, T., Agata, Y., Kanae, S., Saruhashi, T., Yang, D. W., and Musiake, K.: Global assessment of current water resources using total runoff integrating pathways, Hydrolog. Sci. J., 46, 983–995, 2001.

Oki, T. and Kanae, S.: Virtual water trade and world water resources, Water Sci. Technol., 49, 203–209, 2004.

Oki, T. and Kanae, S.: Global hydrological cycles and world water resources, Science, 313, 1068–1072, 2006.

Ramankutty, N. and Foley, J. A.: Characterizing patterns of global land use: An analysis of global croplands data, Global Biogeochem. Cy., 12, 667–685, 1998.

Raskin, P., Gleick, P., Kirshen, P., Pontius, G., and Strzepek, K.: Comprehensive assessment of the freshwater resources of the world, Stockholm Environment Institute, Stockholm, Sweden, 1997.

Shiklomanov, I. A.: Appraisal and assessment of world water re-

sources, Water Int., 25, 11–32, 2000.
Shirakawa, N.: A conceptual framework for global estimation of environmental flow, J. Hydraul. Eng.-JSCE, 48, 421–426, 2004.
Shirakawa, N.: Global estimation of environmental flow requirement based on river runoff seasonality, J. Hydraul. Eng.-JSCE, 49, 391–396, 2005.
Smakhtin, V., Revenga, C., and Doll, P.: A pilot global assessment of environmental water requirements and scarcity, Water Int., 29, 307–317, 2004.
Vörösmarty, C. J., Green, P., Salisbury, J., and Lammers, R. B.: Global water resources: vulnerability from climate change acid population growth, Science, 289, 284–288, 2000.
World Agricultural Outlook Board US Department of Agriculture: Major world crop areas and climatic profile, US Department of Agriculture, Washington DC, USA, 1994.